SMA Memo 156

Version 2: March 26, 2005

Status of the SMA Polarimetry System

D. P. Marrone, R. Rao

1. Introduction

At present, the Submillimeter Array (SMA) is equipped with single, linearly polarized (LP) feeds for each of its three observing bands. In this configuration it is not possible to make polarimetric observations[1], which generally require two orthogonal polarizations to be obtained simultaneously. One solution, recommended in the conclusions of the 1998 SMA polarimetry workshop (Wilner 1998), is to use quarter-wave plates to convert each SMA feed to a switchable circular feed. This technique has been used at the Berkeley-Illinois-Maryland Association array (BIMA) for many years to allow polarimetry. Waveplates and positioning hardware have now been built for the SMA, and has been in use since April 2004. Here we discuss the design of this hardware, the observing procedures, and the measured performance.

2. Polarimetry Hardware

Linear polarization measurements with interferometers are best done with circularly polarized (CP) feeds (see, for example Thompson et al. 2001). This minimizes the effect of gain errors, as the cross-correlation of opposite circular polarizations does not involve the Stokes total intensity (I) parameter. LP to CP conversion is possible through the use of quarter-wave plates, birefringent optical components designed to create a 90° phase delay between LP components along the two crystal axes. By positioning one crystal axis at +45° or −45° to the incident linear polarization, it is possible to obtain left- or right-circular polarization (LCP or RCP).

The SMA polarimetry hardware is shown in Figure 1. The waveplates are held in rotation stages which allow rapid switching between the two positions corresponding to LCP and RCP. The hardware is designed to switch in well under the length of a correlator Walsh cycle (2.58111 s) so that only a single cycle of dead time is needed. This design is different from the system at BIMA, where each antenna has two fixed waveplates for each band. This is largely for historical reasons, the project was originally conceived to make use of just three spare sapphire waveplates that were on hand in 2003. The drawback of this design is the need for highly repeatable angular positioning, but laboratory tests show that positions are reacquired to an accuracy better than the $\sim 0.1°$ we can measure.

[1]In the case of strong, highly-polarized sources or spectral lines, it is possible to measure polarization through parallactic angle rotation, see Shinnaga et al. (2004).

The 340 GHz waveplates used in the SMA are of two different designs. Seven antennas have waveplates made of quartz, with low-density polyethylene (LDPE) anti-reflection (AR) coatings. The LDPE coating ($n = 1.51$) is well matched to the quartz ($n_o = 2.106$, $n_e = 2.154$, the ideal AR coating has an index that is the square root of the substrate index), so the reflection losses and cross-polarization leakages are expected to be small. One waveplate remains from the original set of three sapphire plates. The sapphire has a much larger index of refraction ($n_o = 3.069$, $n_e = 3.403$) so the LDPE is not a perfect AR coating. As is seen in the following sections, the performance of this plate is somewhat degraded. The thickness of the plates is determined by the birefringence, $n_e - n_o$, and the desired optimum frequency. In the case of the quartz plates the birefringence has a large fractional error (0.048 ± 0.005), so the thickness is poorly constrained. Measurements detailed below indicate that the actual waveplates are tuned to within 2% of the desired 342 GHz.

3. Polarimetric Observations

To circumvent the lack of a second feed, polarimetric observations are obtained by switching each antenna between L and R in a coordinated temporal sequence. Using carefully chosen Walsh function modulation for the antenna polarization, it is possible to sample all four combinations of L and R on each baseline (LL, LR, RL, RR) in a short period of time. A cycle of period 16 will provide four samples in each state on each baseline per cycle, with 23 out of the 28 baselines in the full array obtaining all four polarizations every four steps. With all four correlations it is possible to obtain "full" polarimetry, that is, to reconstruct all four Stokes parameters. The data are averaged over the Walsh cycle to produce quasi-simultaneous dual polarization measurements. Beam smearing resulting from this process is negligible.

The quarter-wave plates do not produce pure LCP and RCP, particularly at frequencies away from their design frequency. The feed response is can be modeled by a term representing its sensitivity to the desired polarization plus a fractional sensitivity to the orthogonal polarization, a complex "leakage" term (Sault et al. 1996). In this model the equations governing the response of the interferometer can be linearized with a few assumptions, allowing easy calculation of the leakage terms. The leakages can be calibrated using by observing a source of unknown (but non-zero) polarization over a large range of parallactic angles, because the leakage-induced polarization is constant through the track while the source polarization rotates relative to the feed as it moves across the sky. This technique is essential for the data reduction, but it also provides a check on the properties of our polarization system.

4. Verification of Polarized Leakages

4.1. Theoretical Leakages

The leakages of the L and R feeds can be predicted based on an understanding of the imperfections in the waveplates. There are three types of imperfections affecting our leakages to varying degrees. The first is that the quarter-wave plates only generate a $\lambda/4$ retardation at one $\lambda_0 = c/\nu_0$, that is, the retardation is constant (in path length units) and cause a phase delay equal to the path delay divided by the wavelength. We can parameterize this imperfection as $\delta = (\pi/2)(\nu/\nu_0 - 1)$, the deviation from a phase delay of $\pi/2$, given a nominal frequency ν_0. The second effect is that the waveplate axes may not be positioned at $\pm 45°$ to the feed polarization, but may deviate from this by some angle θ. Unlike δ, θ may differ between the L and R polarization states on a given antenna because they correspond to two different positions of the waveplate rotation stage and these are aligned separately. The final effect is the difference between the reflectivity of the waveplate in the two crystal axes. The difference in the index of refraction in the crystal along two axes generates the delay between the polarization states, but it also creates a difference in reflectivity. The transmissivity of polarizations aligned with the ordinary and extraordinary axes can be related by $T_e = T_o\,(1 + \epsilon)$. This correction can vary significantly with frequency and can change sign between sidebands.

Following the formalism set out in Hamaker et al. (1996), we can express the leakage of RCP into the LCP feed as (Rao 1999):

$$d_R = \frac{e^{2i\theta}\left[e^{i\delta/2}\left(1 + ie^{2i\theta}\right) - (1+\epsilon)\,e^{-i\delta/2}\left(i + e^{2i\theta}\right)\right]}{e^{i\delta/2}\left(-i + e^{2i\theta}\right) + (1+\epsilon)\,e^{-i\delta/2}\left(1 - ie^{2i\theta}\right)} \tag{1}$$

For small δ, θ, and ϵ, to first order the leakages should be:

$$d_R = -\frac{\delta}{2} - i\left(\theta + \frac{\epsilon}{2}\right) \tag{2}$$

As pointed out in Rao (1999), the first term shows that the real component of the leakage should be linear with frequency and given by $Re[d_R] = -(\pi/4)(\nu/\nu_0 - 1)$. To first order, we should have $d_R = d_L$ for a given waveplate. The imaginary part of the leakage can be used to determine the alignment error (θ) for $\epsilon = 0$, but in practice this term is significant enough to affect the results even for the well matched quartz waveplates. Since the epsilon contribution should be the same for d_R and d_L, their imaginary components can be combined to give:

$$Im\left[d_R - d_L\right] = -\left(\theta_R - \theta_L\right) \tag{3}$$

where the two angles are the errors in the positions of the two states. This difference represents the deviation from the nominal 90° switch.

4.2. Measured Leakages

Leakages have been obtained at four frequencies (two tunings, two sidebands), with two measurements per tuning. On May 25 and July 14, 2004 leakages were determined at 331.7 and 341.7 GHz, and on December 5 and 6 at 335.8 and 345.8 GHz. On some of these nights, combinations of antennas 4, 7, and 8 were missing from the array, so only antennas 1, 2, 3, 5, and 6 have leakages at all four frequencies.

Figure 2 shows the real part of the leakages obtained at each frequency for each antenna. The d_R and d_L have been averaged together at each frequency, as have the two measurements of each leakage. As described above, $Re[d_R]$ and $Re[d_L]$ are the same to first order, and the expected slope of $Re[d]$ with ν is $\pi/(4\nu_0)$. For the four antennas with leakages at all frequencies (antenna 3 is excluded because it uses a sapphire waveplate), the best fit to the real part of the average leakages is given by $d = -0.0021(\nu - 348.0)$. This slope is quite close to the expected -0.00225 for the measured optimal frequency of 348.0 GHz. Antenna 3 stands out from the rest because of its sapphire waveplate. The AR coating on this plate is not well matched to the higher index of the sapphire, so the reflection is much higher, and the larger difference between the ordinary and extraordinary indices of refraction gives substantial ϵ, as large as 15%. To second order, $Re[d_R] = -\delta/2 + \epsilon\theta$, so the large slope is likely due to the combination of ϵ and a non-zero alignment error, although the exact shape of the $\epsilon - \nu$ curve depends on the coating thickness.

The variation in the leakages from night-to-night is shown in Figures 3 and 4. Figure 3 shows the two individual measurements of $Re[d_R]$ (ends of error bars) at each frequency, with the average of the two plotted as a line. The variability in the measurements does not necessarily mean that the leakages themselves are varying from installation to installation, instead, this may be due to the signal to noise obtained on 7/14 and 12/6 when τ_{225} was around 0.1. Figure 4 shows the rms of the four $Re[d]$ measurements (d_R and d_L) for each antenna. The rms is at or below 1% for all antennas except 7, which shows very strange results on 7/14.

The imaginary components of the leakages should be independent of frequency in the absence of a large ϵ, as can be seen in equation 2. For our quartz waveplates and LDPE AR coatings, the expected value of $|\epsilon|$ is no more than 1%, although it depends sensitively on the coating thickness and is more typically $0-0.5\%$. The values of $Im[d_R]$ for each antenna at all the available frequencies are plotted in Figure 5. This term appears to be fairly independent of frequency, except in the case of antenna 3. Assuming that the ϵ term is unimportant (a poor assumption), this indicates that the position error in the L state in each antenna is about 1° in the worst case (antenna 4). Differencing the d_R and d_L leakages to eliminate ϵ, we obtain Figure 6. Again, we find that the deviation from the nominal 90° switch is no worse than 1°, with most antennas showing very small errors. Antenna 3 shows some deviation from flatness with frequency, but most antennas have constant $Im[d_R - d_L]$, as expected.

In all, the waveplate leakages are behaving as expected from simple theoretical considerations. This gives us confidence in both our ability to measure these leakages and the applicability of

leakages measured on one night to data taken on another. It is still difficult to determine the level at which the leakages vary from night to night or from installation to installation as we have very little leakage data. These two possibilities can be examined, to some extent, with the current data, as the 331.8 and 341.8 GHz leakages were obtained on widely separated nights while the other two frequencies were measured on consecutive nights without removing the waveplates. Looking again at Figure 4, the rms on the 331.8 and 341.8 GHz points (first and third points at each antenna) is not systematically larger than it is on the points measured on consecutive nights (335.8 and 345.8, second and fourth). The degree to which the leakage measurement error (or the as of yet unquantified variability) affects the results we obtain is discussed in an example in the following section.

5. Other Astronomical Tests

Absolute calibration of the polarization system is difficult to achieve because we lack a calibrator of known polarization fraction and position angle. We have devised some sanity checks to ensure that the polarization observations do not produce unreasonable results.

5.1. Source with Known Polarization

Of particular concern is the possibility that we have swapped the L and R labels for the polarization states. Although we have carefully considered the polarization inversions caused by the SMA optics, it is important to confirm our conclusions with an astronomical test. The effect of swapping L and R (in the case of ideal waveplates) is to multiply Stokes U and V by -1, which replaces the polarization position angle (PA) by 180−PA. In practice, the difference between the leakages determined in the two cases can cause the position angle to deviate from this simple result.

Of the sources we have observed to date, the one with the best known PA is NGC 1333 IRAS 4A, where the dust polarization has also been mapped with BIMA (Girart et al. 1999). Figure 7 shows a comparison of the polarization obtained at 230 GHz with BIMA and 340 GHz with the SMA. Note that the SMA beam is much smaller, clearly resolving the two continuum peaks in this multiple source, and providing much more information about the polarization distribution. The PA found in Girart et al. (1999) at the peak of the intensity map is $146^\circ \pm 7^\circ$, while the SMA data indicates $143.0^\circ \pm 1.6^\circ$, after smoothing to the same beam. If L and R are swapped we obtain $44.3^\circ \pm 2.4^\circ$(not far from $180 - 143$), so it appears likely that we have correctly labeled the polarization states.

5.2. Unpolarized Source

A simple check of the leakages can be obtained by applying them to an unresolved and unpolarized source, such as Ganymede. In the December 2004 polarization observations of NGC 1333, Ganymede was used as a flux calibrator. It was imaged with and without the application of leakage solutions, and the polarization properties of the images are reported in Table 1. The results in the table are the combined results from December 5 and 6, and P is the LP fraction: $P = \sqrt{Q^2 + U^2}$. The sidebands are centered on 345.8 and 335.8 GHz; both are below the optimal frequency of the (non-sapphire) waveplates. As the LSB is much further from this frequency, the polarization signal is larger before leakages are applied. The polarization is completely eliminated in the LSB (below 2σ), while it is largely unchanged in the USB, although it is below the noise level in the I map and only 3σ in the P map.

5.3. Effects of Leakages on Measured Polarization

The leakages seem broadly consistent from measurement to measurement, as was shown in § 4.2. Nevertheless, since the leakages vary at the 1% level from measurement to measurement, it is important to know the effect the leakage variations have on the polarization we measure. Using the leakages determined on May 25 and July 14, we measured the polarization of 3c279 in the May 25 data (note that this source was also the leakage calibrator in this track). We have chosen this data because of its extremely high signal to noise. The leakages from both days were applied to the data separately, keeping only the antennas common to both (1-7). The derived polarization properties are given in Table 2. The polarization is quite different with and without leakages, but the values measured with the two leakage solutions are quite similar. The polarization fractions of both sidebands do decrease when using the July 14 leakages, but the difference is just barely significant, while the PA (χ) change is within the level of the errors. Note that the two sidebands agree better with the May 25 leakages than with the July 14 leakages. The same test applied to the July 14 leakage calibration data (not shown) also results in better agreement using the May 25 leakages, so we suspect that the origin of these differences is a poor leakage solution obtained in bad weather on July 14. More leakage data was obtained on March 24, 2005 and is currently being reduced. This data is of higher quality than the July 14 data and should shed light on leakage variability. In any case, it appears that the choice of leakage solution is not very important, even in this high signal to noise data.

6. Future Upgrades

The SMA polarization system is currently being upgraded to include a new set of waveplates. By May, polarimetry will be possible with the current 340 GHz waveplates, as well as with a new set of waveplates for simultaneous polarimetry at 230 and 690 GHz. These new waveplates rely on

the convenient factor of three spacing between these two bands to operate as normal quarter-wave plates at 230 GHz and three-quarter-wave plates at 690 GHz, both of which serve to convert LP to CP. The sets of waveplates will be interchangeable, so that observations with the two sets can be made on consecutive nights.

On a longer timescale, the waveplate positioning system will be included in the new calibration load system, so that the plates can be automatically moved into and out of the beam. Even with dual polarization feeds planned for the 345 GHz band, polarimetry will still require waveplates to generate the CP feeds preferred for detection of linear polarization. Moreover, as the other two bands currently in use are not slated to be paired with cross-polar feeds, polarimetry at other frequencies will always require switching waveplates. By mounting the waveplates on the calibration load system, they should be easily incorporated into normal SMA observations.

REFERENCES

Girart, J. M., Crutcher, R. M., & Rao, R. 1999, ApJ, 525, L109

Hamaker, J. P., Bregman, J. D., & Sault, R. J. 1996, A&AS, 117, 137

Rao, R. 1999, Ph.D. Thesis, http://cfa-www.harvard.edu/∼rrao/thesis.ps

Sault, R. J., Hamaker, J. P., & Bregman, J. D. 1996, A&AS, 117, 149

Shinnaga, H., Moran, J. M., Young, K. H., & Ho, P. T. P. 2004, ApJ, 616, L47

Thompson, A. R., Moran, J. M., & Swenson, G. W. 2001, Interferometry and synthesis in radio astronomy (New York : Wiley)

Wilner, D. 1998, Polarimetry with the SMA: Workshop Summary, SMA Memo 129, Smithsonian Astrophysical Observatory

This preprint was prepared with the AAS LaTeX macros v5.2.

Table 1. Polarization results on Ganymede

	USB Raw	LSB Raw	USB Leakages	LSB Leakages
I_{peak} (Jy)	3.71±0.03	3.87±0.03	3.70±0.03	3.86±0.03
P_{peak} (mJy)	27±9	184±9	26±8	<15
P (%)	0.7±0.2	4.8±0.2	0.7±0.2	<0.4

Table 2. May 25 polarization results on 3c279 for various leakage solutions

Leakages	USB None	LSB None	USB 5/25	LSB 5/25	USB 7/14	LSB 7/14
I (Jy)	6.601±0.015	6.919±0.017	6.601±0.015	6.910±0.016	6.602±0.015	6.911±0.017
P (mJy)	168±8	229±15	222±6	252±7	200±7	235±9
P (%)	2.5±0.1	3.3±0.2	3.4±0.1	3.6±0.1	3.0±0.1	3.4±0.1
χ (°)	44±1	34±2	45.1±0.7	46.7±0.8	45.0±1.0	48.4±1.0

Note. — I and P errors are the rms noise in the individual maps, not the overall uncertainty in the flux scale.

Fig. 1.— The SMA polarimetry hardware. The eight waveplates and positioning stages are in the foreground. These motor driven rotation stages allow rapid switching between LCP and RCP. Behind them are the eight control assemblies containing computers and power supplies.

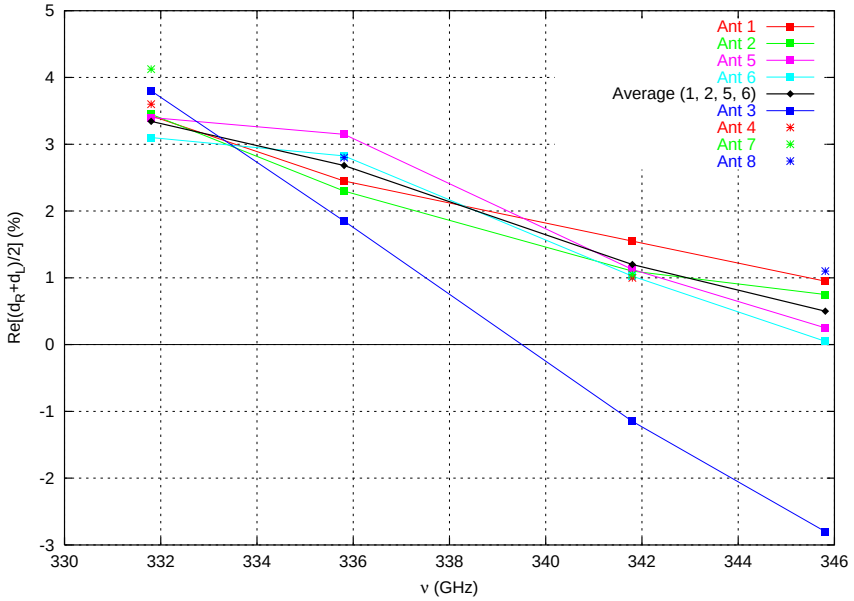

Fig. 2.— Average $Re[d]$ for all antennas. The four antennas with complete measurements and quartz waveplates (1, 2, 5, 6) have also been averaged together and plotted in black. The best fit to this average leakage curve is $d = -0.0021(\nu - 348.0)$.

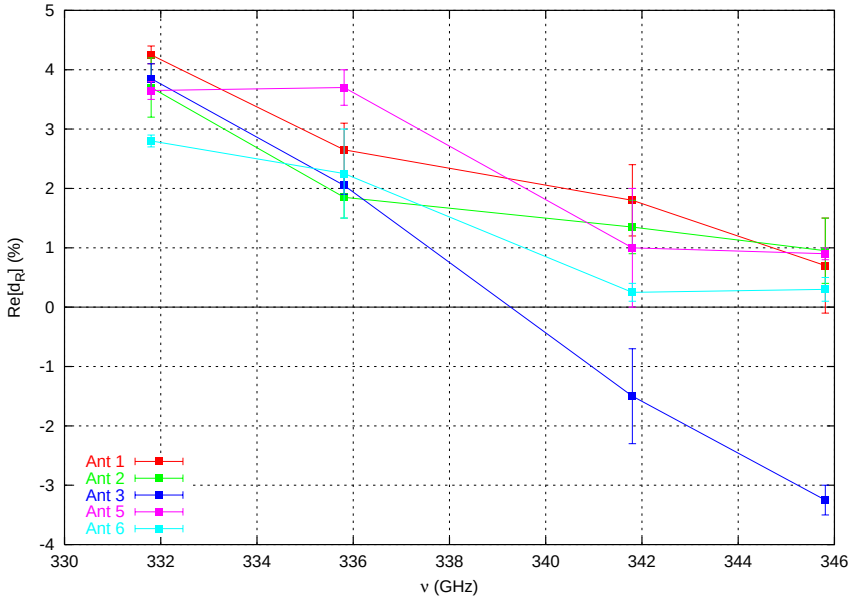

Fig. 3.— Variations in the measured $Re[d_R]$. For each of 5 antennas the two measurements at each frequency are shown as the upper and lower ends of the error bars; the average of the two is drawn as a line.

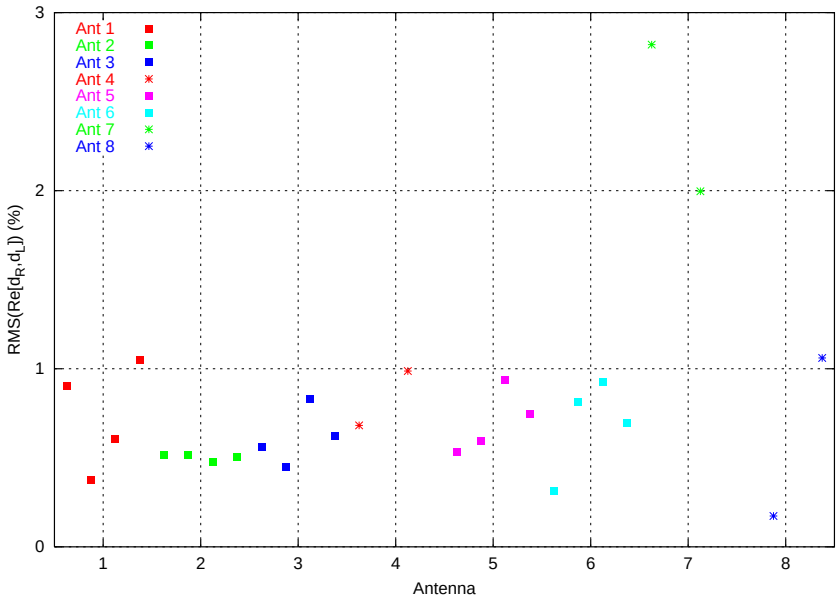

Fig. 4.— The rms variation of the four measurements (two dates, d_R and d_L) of $Re[d]$ for each antenna at each frequency. The frequencies increase to the right in each set of points.

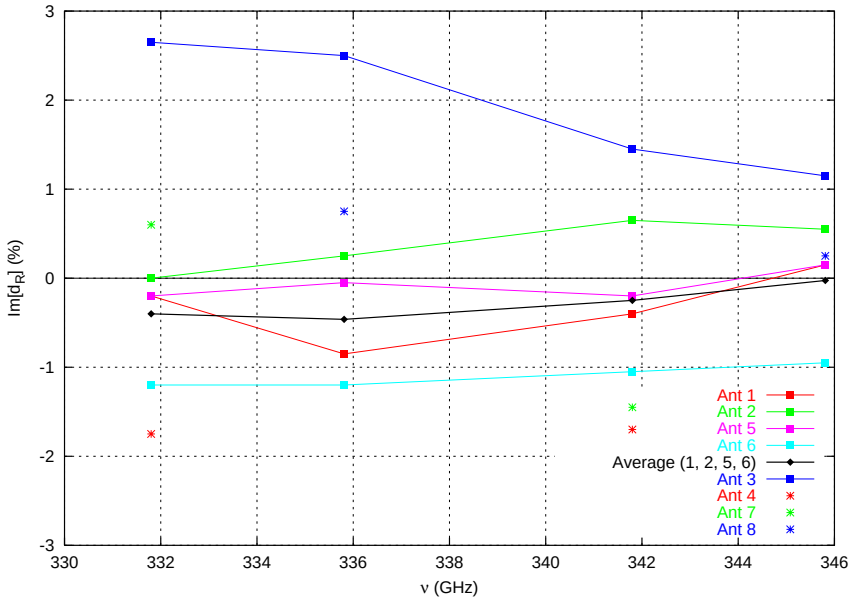

Fig. 5.— $Im[R]$, averaged over the two measurements at each frequency. The average for the four usual antennas is also plotted, showing that there is little average trend with frequency.

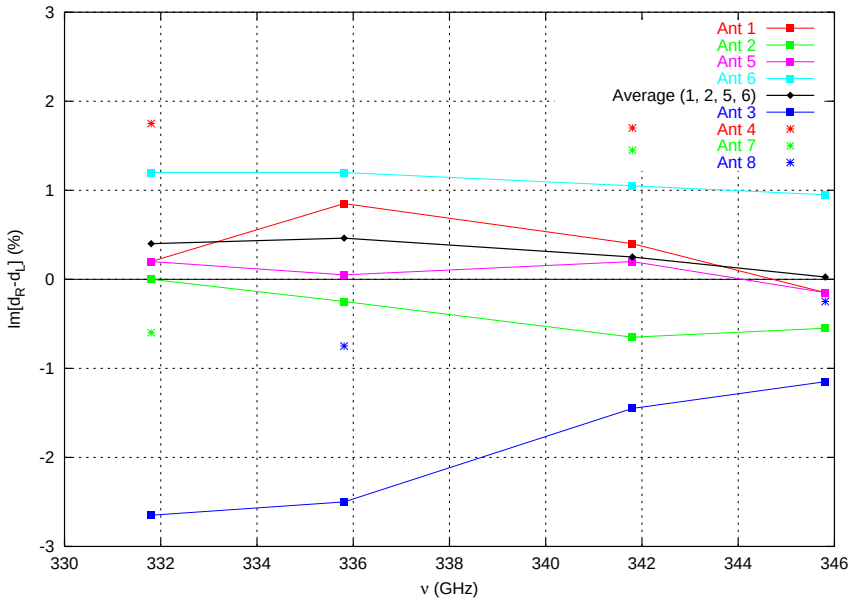

Fig. 6.— The difference between the imaginary parts of d_R and d_L. This quantity should be independent of frequency and represent the error in the switching angle, where 1% represents 0.57°. For all antennas this error seems to be less than 1°. Antenna 3 again stands out.

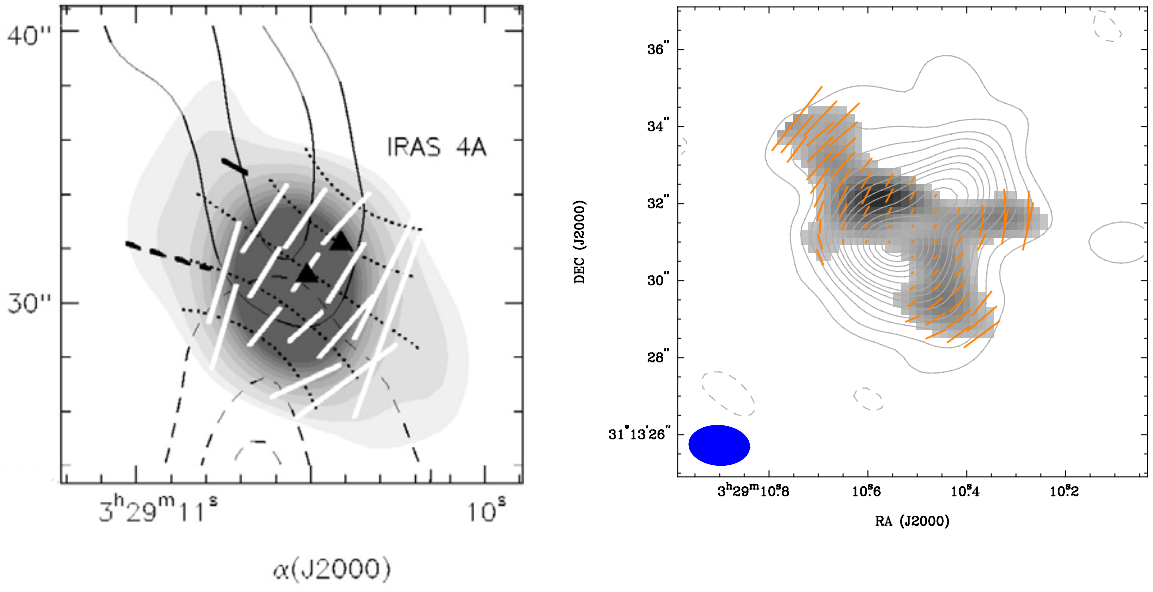

Fig. 7.— Dust polarization maps of NGC 1333 IRAS4A at 230 GHz (*Left*; Girart et al. 1999) and 340 GHz (*Right*; Rao et al., in preparation). The beams are $4\farcs4\times2\farcs8$ and $1\farcs5\times1\farcs0$, respectively. *Left*: Stokes I is plotted in greyscale with polarization fraction and direction plotted as vectors. *Right*: Stokes I is contoured, with the linearly polarized flux in greyscale, and polarization fraction and direction as vectors. Vector scales are not equal between the plots.